Structural state of relaxor ferroelectrics $PbSc_{0.5}Ta_{0.5}O_3$ and $PbSc_{0.5}Nb_{0.5}O_3$ at high pressures up to 30 GPa

B. J. Maier,[1] N. Waeselmann,[1] B. Mihailova,[1,*] R. J. Angel,[1,2,†] C. Ederer,[3] C. Paulmann,[1] M. Gospodinov,[4] A. Friedrich,[5] and U. Bismayer[1]

[1]*Department Geowissenschaften, Universität Hamburg, D-20146 Hamburg, Germany*

[2]*Crystallography Laboratory, Department of Geosciences, Virginia Tech, Blacksburg, Virginia 24060, USA*

[3]*School of Physics, Trinity College, Dublin 2, Ireland*

[4]*Institute of Solid State Physics, Bulgarian Academy of Sciences, Boulevard Tzarigradsko Chausse 72, BG-1784 Sofia, Bulgaria*

[5]*Institut für Geowissenschaften, Goethe-Universität, Altenhöferallee 1, D-60438 Frankfurt am Main, Germany*

(Received 6 July 2011; revised manuscript received 15 October 2011; published 7 November 2011)

The pressure-induced structural changes in perovskite-type (ABO_3) Pb-based relaxor ferroelectrics are studied on the basis of *in situ* single-crystal synchrotron x-ray diffraction and Raman scattering experiments on $PbSc_{0.5}Ta_{0.5}O_3$ and $PbSc_{0.5}Nb_{0.5}O_3$ conducted under hydrostatic conditions up to 30 GPa. Complementary density functional theory calculations have been performed to compare the stability of various atomic configurations for both compounds at high pressures. By combining the experimental and theoretical results, the following sequence of structural transformations is proposed. At a characteristic pressure $p_1^\star$ the mesoscopic polar order is violated and a local antipolar order of Pb atoms as well as quasidynamical long-range order of antiphase octahedral tilts is developed. These structural changes facilitate the occurrence of a continuous phase transition at $p_{c1} > p_1^\star$ from cubic to a nonpolar rhombohedral structure comprising antiphase octahedral tilts of equal magnitude ($a^-a^-a^-$). At a characteristic pressure $p_2^\star > p_{c1}$ the octahedral tilts around the cubic [100], [010], and [001] directions become different from each other on the mesoscopic scale. The latter precedes a second phase transition at p_{c2}, which involves long-range order of Pb antipolar displacements along cubic [uv0] directions and a compatible mixed tilt system ($a^+b^-b^-$) or long-range ordered antiphase tilts with unequal magnitudes ($a^0b^-b^-$) without Pb displacement ordering. The phase-transition pattern at p_{c2} depends on the fine-scale degree of chemical B-site order in the structure.

DOI: 10.1103/PhysRevB.84.174104 PACS number(s): 77.80.Jk, 64.70.Nd, 63.20.−e, 71.15.Nc

I. INTRODUCTION

Lead-based perovskite-type (ABO_3) relaxor ferroelectrics possess a remarkably high frequency-dependent dielectric permittivity and exceptional piezoelectric, electro-elastic, and electro-optic properties[1] at room temperature. Hence they play an important role in a number of technological applications[2] and have challenged the scientific community over the past decades to better understand the atomistic origin of their unique properties. Although the proper theoretical approach is still controversial,[3–8] it is experimentally established that their properties are related to their structural complexity on the mesoscopic scale,[1,9,10] i.e., dynamic polar nanoregions (PNRs) embedded in a nonpolar matrix, that flip between different orientation states on the microsecond time scale.[11] These dynamic PNRs nucleate by coupling of randomly off-centered cation shifts[12] at the Burns temperature T_B,[13] which is several hundred kelvins above the frequency-dependent temperature of the dielectric permittivity maximum T_m. At $T^\star$, a recently established intermediate temperature characteristic of relaxors,[12,14–16] the preexisting polar clusters merge into larger polar clusters with slower dynamics. Below T_m, the PNRs become static at the freezing temperature T_f for canonical relaxors or they develop into normal ferroelectric domains that exhibit a very weak ferroic distortion of the unit cell. The driving mechanism for the existence of PNRs is still under discussion. Numerous publications on the topic show that substitutional disorder on the A and/or B site enhances the relaxor state in perovskite-type ferroelectrics. Hence random local electric and/or elastic fields play an important role in the formation and development of PNRs. A coexistence of polar and anti-ferrodistortive order in lead-based relaxors was also proposed to be a cause for the relaxor behavior.[17–20]

Various experimental methods have been applied in order to resolve the structural complexity of relaxors. Structural studies under high pressure are of particular importance because pressure may enhance ferroic structural species present at ambient conditions along with PNRs, but which are not favored by a temperature decrease. Recently, by combining high-pressure synchrotron single-crystal x-ray diffraction (XRD), powder neutron diffraction, and Raman spectroscopy on a series of pure, A-site-, and B-site-doped $PbSc_{0.5}Ta_{0.5}O_3$ (PST) and $PbSc_{0.5}Nb_{0.5}O_3$ (PSN), we demonstrated that pressure induces a continuous cubic-to-rhombohedral phase transition associated with the development of an antiphase octahedral tilt pattern of type $a^-a^-a^-$ (Glazer's notation[21]) and the suppression of polar B-cation displacements.[22] The critical pressure p_c at which the cubic symmetry of the average structure is broken is preceded by an intermediate pressure $p^\star$ at which the coupling between off-centered Pb and B-site cations in PNRs is suppressed and local ferroic order of Pb cations as well as quasidynamical long-range order of antiphase BO_6 tilts detectable by neutron diffraction is developed. Thus, the complementary phonon spectroscopic and diffraction analyses reveal that pressure suppresses the polar intermediate-range order and favors the anti-ferrodistortive long-range order, which is developed from ferroic Pb-O species already existing at ambient conditions.[22]

 ©2011 American Physical Society

Copyright by the American Physical Society. Maier, B. J. ; Waeselmann, N. ; Mihailova, B. ; et al., Nov 7, 2011. "Structural state of relaxor ferroelectrics PbSc0.5Ta0.5O3 and PbSc0.5Nb0.5O3 at high pressures up to 30 GPa," PHYSICAL REVIEW B 84(17): 174104. DOI: 10.1103/PhysRevB.84.174104.

On the basis of combined XRD and Raman scattering studies of $PbZn_{1/3}Nb_{2/3}O_3$ (PZN) up to 46 GPa Janolin *et al.*[23] proposed the following pressure-induced phase transition sequence: polar $R3m \xrightarrow{p_{c1}}$ nonpolar $R\bar{3}c \xrightarrow{p_{c2}}$ nonpolar $C2/c \xrightarrow{p_{c3}}$ polar Cc. The first transition near 5 GPa was revealed by the appearance of pressure-induced superstructure reflections with h,k,l, all odd (Miller indices are given with respect to $Fm\bar{3}m$ throughout this paper) consistent with an antiphase tilting $a^-a^-a^-$ and is similar to the continuous pressure-induced phase transition that has been found in many other Pb-based perovskite-type relaxors.[22,24] The second pressure-induced phase transition in PZN was assumed to be near 10 GPa on the basis of anisotropic distortion of the unit cell as well as substantial broadening of the Bragg diffraction peaks, both inconsistent with cubic or rhombohedral symmetry.[23] The third transition at 23 GPa was deduced from changes in the Raman spectra and a polar space group was proposed by analogy with the structural state of $PbTiO_3$ at very high pressures.[25] It should however be emphasized that the *in situ* high-pressure experiments on PZN were carried out in argon as a pressure-transmitting medium,[23] which above 2 GPa is nonhydrostatic[26] and above 10 GPa the degree of nonhydrostaticity is considerable.[27] This might substantially change both the phases observed and the transitions between them.

The aim of this paper is to verify the occurrence of further phase transitions in lead-based perovskite-type relaxors, above the continuous phase transition involving long-range BO_6 antiphase tilting. For this purpose we have chosen to study pure PST and PSN in the pressure regime up to 30 GPa, since these two compounds have been thoroughly studied in the low-pressure regime by single-crystal in-house and synchrotron XRD, neutron powder diffraction, and single-crystal Raman spectroscopy.[28–32] We applied high-pressure single-crystal synchrotron XRD and simultaneous off-beam Raman spectroscopy to the same specimens, using He as a pressure-transmitting medium, which is hydrostatic up to 20 GPa[27] and between 20 and 30 GPa exhibits a negligible degree of deviation from hydrostaticity as compared to the other commonly used pressure-transmitting media.[27] In addition, we performed density functional theory (DFT) calculations for PST and PSN to determine the energetically preferred octahedral tilt patterns at high pressures and to check whether polar or nonpolar structures are favored by high pressure.

II. EXPERIMENTAL DETAILS

Cube-shaped single crystals of $PbSc_{0.5}Ta_{0.5}O_3$ and $PbSc_{0.5}Nb_{0.5}O_3$ of optical and chemical homogeneity were synthesized by the high-temperature solution crystal growth method. The chemical composition was verified by electron microprobe analysis (Cameca microbeam SX100 SEM system), by averaging over 100 spatial points on each sample.

Specimens of approximate size $80 \times 80 \times 30\ \mu m^3$ for PST and $60 \times 30 \times 20\ \mu m^3$ for PSN were cut from polished {100} plates. The same single-crystal specimens were probed by high-pressure synchrotron XRD and Raman spectroscopy, using diamond anvil cells of the Boehler-Almax type[33] and helium as a pressure-transmitting medium. The diameter of the diamond culets was 600 and 500 μm for PST and PSN, respectively. Rhenium gaskets of 200 μm thickness preindented to $\sim$65 μm were drilled with a spark eroder to form a sample chamber hole with a diameter of 220 and 180 μm for PST and PSN, respectively. During the He gas-loading procedure, the diameter of the gasket holes shrank respectively to 140 and 100 μm due to the initial gas compression. The ruby-line luminescence method[34] was used to determine pressure with an uncertainty of $\sim$0.1 GPa in the low-pressure regime and $\sim$0.2 GPa in the high-pressure regime. The pressure magnitude and hydrostaticity was also double-checked by following the photoluminescence peak position and width of Sm^{2+}-doped SrB_4O_7.[35]

Single-crystal synchrotron XRD experiments were conducted at the DESY/HASYLAB F1 beamline using a MarCCD 165 detector, a radiation wavelength of $\lambda = 0.5000$ Å, a sample-to-detector distance of 100 mm, and a step width of 0.5° per frame. The exposure time per frame was 120 s for PST and 360 s for PSN.

Off-beam Raman spectra in the wave number range 15–1200 cm^{-1} were collected in backscattering geometry with a Horiba Jobin-Yvon T64000 triple-grating spectrometer equipped with an Olympus BH41 microscope and a 50 × long-working-distance objective, using the 514.5-nm line of an Ar^+ laser. The spectral resolution was 2 cm^{-1}, while the lateral resolution on the sample surface was 2 μm. Spectra from several spatial areas were collected at each pressure to check whether the samples remained structurally homogeneous at high pressures. Additionally, at each pressure a background spectrum from the sample chamber was recorded under the same experimental conditions as the sample spectrum and subsequently subtracted from the sample spectrum in order to eliminate possible artificial signals. Then the sample spectra were reduced by the Bose-Einstein phonon occupation factor to eliminate the effect of temperature on the peak intensities and fitted with Lorentzian functions to determine the peak positions, full widths at half maximum (FWHMs), and intensities.

XRD and Raman scattering measurements on decompression confirmed the reversibility of the observed pressure-induced structural changes. For PST, which at high pressures showed inhomogeneity with respect to the Raman signals below 110 cm^{-1}, Raman mapping with a lateral step of 2 μm was performed on decompression. The total acquisition time for a single Raman map was approximately 28 h, which prohibited mapping on pressure increase because of time restrictions during the beamtime period at DESY/HASYLAB.

III. COMPUTATIONAL DETAILS

Total energy calculations using density functional theory within the local density approximation[36] have been performed for both PST and PSN with perfect chemical rocksalt-type ordering on the perovskite B site. In order to identify possible structural transitions under external pressure, we have initialized atomic positions according to different tilt systems with different space group symmetries. Both atomic positions and unit-cell vectors have then been relaxed at fixed volume until the forces were smaller than 10^{-3} eV/Å. Similar calculations have been performed at different volumes. The following tilt-systems (space group symmetries) have been

considered: $a^0a^0a^0$ ($Fm\bar{3}m$), $a^-a^-a^-$ ($R\bar{3}$), $a^0a^0c^-$ ($I4/m$), $a^0b^-b^-$ ($C2/m$), $a^-b^-b^-$ ($P\bar{1}$), and $a^+b^-b^-$ ($P2_1/c$). In addition, two polar symmetries corresponding to tilt systems $a^-a^-a^-$ ($R3$) and $a^0b^-b^-$ ($C2$) have been considered. In these cases additional shifts along the polar direction have been applied to the initial atomic positions.

All calculations have been performed using the Vienna *Ab initio* Simulation Package (VASP) and the projector augmented wave method.[37–39] The following semicore states, corresponding to completely filled electronic shells, have been included in the valence for better accuracy: Pb $5d$, Sc $3p$ and $3s$, Nb $4p$, and Ta $5p$. The Ta $4f$ states have been frozen into the core potential. A plane wave energy cutoff of 550 eV was used and convergence of the total energy with respect to k-point sampling was tested to be better than 1 meV for all considered structures.

IV. RESULTS AND DISCUSSION

A. Chemical order and structural changes at low pressures

PST and PSN have the same stoichiometry of type $PbB^{3+}_{0.5}B^{5+}_{0.5}O_3$ and the same tolerance factor $t = \frac{r_i(A)+r_i(O)}{\sqrt{2}[r_i(B)+r_i(O)]}$, where r_i stands for the ionic radius, because octahedrally coordinated Ta^{5+} and Nb^{5+} have the same ionic radius.[40] Both compounds may exhibit 1:1 B-site chemical long-range order (rocksalt-type), which consists of alternating B^{3+} and B^{5+} cations along the cubic ⟨100⟩ directions. The degree of chemical B-site order (CBO) can be quantified using the Bragg reflection intensities in powder XRD patterns as the ratio $S = Q_{\text{experimental}}/Q_{\text{theoretical}}$ with $Q = I(111)/I(200)$. Bragg peak indices are given with respect to $Fm\bar{3}m$, which is the symmetry of the perovskite-type cubic structure if the B-site cations are completely ordered.[41] The degree of CBO can also be determined from the site occupation factors (SOFs) of the (4a) or (4b) Wyckoff position in $Fm\bar{3}m$ as equal to $S = |\text{SOF}(B^{3+}) - \text{SOF}(B^{5+})|/|\text{SOF}(B^{3+}) + \text{SOF}(B^{5+})|$. The degree of long-range CBO in both PST and PSN samples studied is very low. For PST $S = 0.13$ with a mean size of the chemically ordered domains ∼6 nm, according to the Bragg intensity ratio from powder XRD, and $S = 0.08$, according to SOFs derived from structure refinements to single-crystal synchrotron XRD data.[12,30] The powder XRD pattern of PSN does not show any superlattice Bragg peaks with h,k,l, all odd, related to CBO.[42] Very weak CBO superlattice reflections were detected only from single crystals measured with synchrotron XRD in air, but not in a diamond anvil cell, which confirms the very low degree of long-range CBO in PSN. However, it should be emphasized that PST and PSN, as all Pb-based B-site complex perovskite-type relaxors, appear chemically ordered on the local scale, because the high-temperature Raman spectra correspond to the double-perovskite $Fm\bar{3}m$ structure and cannot be interpreted in terms of single-perovskite structure.[43,44] The Raman scattering results are in good accordance with x-ray absorption spectroscopic analysis, clearly showing the predominance of B′-O-B″ linkages in Pb-based B-site complex perovskite-type relaxors, regardless of the degree of long-range chemical order.[45] Therefore, it would be more realistic to consider the state of chemical 1:1 B-site order as frustrated CBO, a structural state in which B′-O-B″ linkages dominate but with the long-range order destroyed by a high density of translation-symmetry (e.g., antiphase stacking) faults. This is fundamentally different from the commonly accepted view of the structure as comprising chemically ordered domains in a chemically disordered matrix.

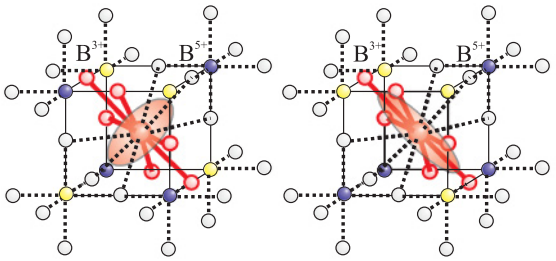

FIG. 1. (Color online) A sketch of $PbB^{3+}_{0.5}B^{5+}_{0.5}O_3$ compound with local chemical 1:1 B-site order (left-hand side) and disorder (right-hand side). The reddish ellipses represent the anisotropic displacement ellipsoids of Pb^{2+} cations.

At ambient pressure and room temperature both samples exhibit a relaxor state, with abundant polar nanoregions which give rise to x-ray diffuse scattering along the cubic reciprocal-space ⟨110⟩* directions.[12,42] According to our previous high-pressure studies, the critical pressure p_{c1} of the continuous cubic-to-rhombohedral phase transition involving $a^-a^-a^-$ tilting is 1.9 GPa for PST and 4.1 GPa for PSN, while the preceding pressure $p^\star$ is 1.2 GPa for PST and 2.5 for PSN.[28–32] The change in the bulk modulus ΔK at p_{c1} is 44.5 GPa for PST and 15.6 GPa for PSN. The jump of K at p_{c1} is a combined result of the actual structural difference between the two phases as well as the material volume involved in the phase transition. Thus, the magnitude of ΔK indicates a higher degree of the overall structural distortion at p_{c1} for PST as compared to PSN. Rietveld refinements to neutron powder diffraction revealed that above $p^\star$ the anisotropic displacement ellipsoids of Pb are elongated along the cubic body diagonal for PST, whereas in the case of PSN they are shaped like flattened disks parallel to the cubic {111} planes.[30,32] The existence of a preferred direction of Pb off-centering suggests that in PST there might be some degree of local order of off-centered Pb displacements at $p > p^\star$. We attribute the observed difference in Pb off-centering in PST and PSN to the fine-scale difference in the abundance of coherent B^{3+}-O-B^{5+} linkages, being larger for PST as compared to PSN. The local chemical B-site order would facilitate the correlation between Pb^{2+} cations shifted along the cubic {111} directions due to electrostatic interactions, while the presence of underbonded oxygen atoms in the case of local chemical disorder would favor Pb^{2+} cations to shift randomly along the cubic ⟨110⟩ directions, i.e., within a plane perpendicular to the cubic body diagonal (see the sketch in Fig. 1). In addition, Raman spectroscopy indicates that even at ambient conditions the ferroic Pb-O species that are enhanced at high pressure have a longer length of coherence for PST as compared to PSN.[12,42,43]

B. The structural state of PST up to 30 GPa

Figure 2 shows reciprocal-space layer sections reconstructed in $Fm\bar{3}m$ from single-crystal synchrotron XRD on PST at different pressures. At 5.0 GPa the crystal is in the

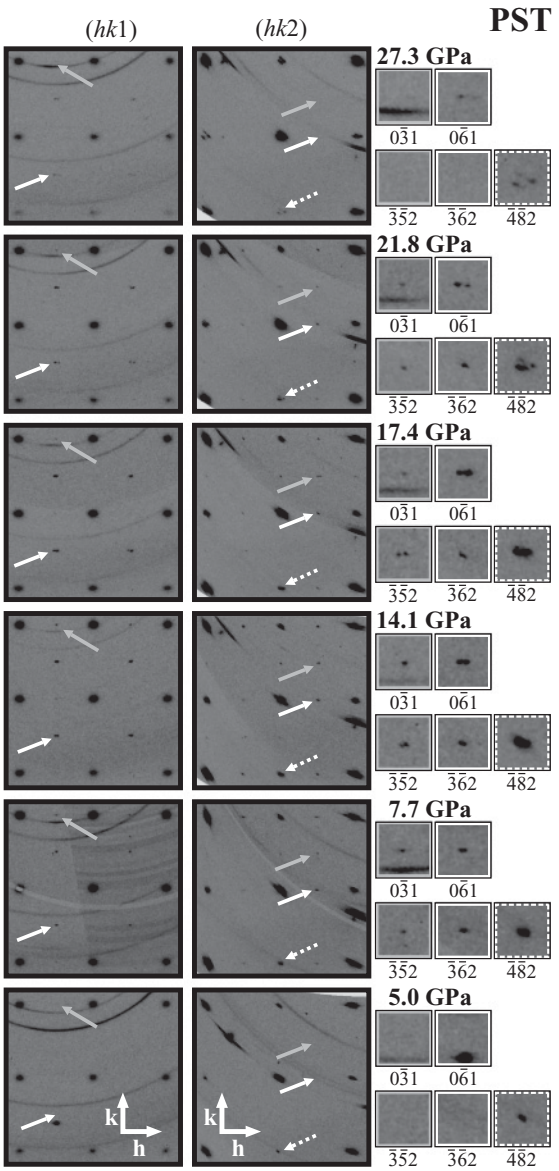

FIG. 2. Reciprocal-space layer sections of PST reconstructed in $Fm\bar{3}m$ from single-crystal synchrotron XRD data. The reflection in the upper-left and lower-right corners are $\bar{1}\bar{3}1$ and $3\bar{7}1$ for the ($hk1$) layer and $\bar{6}\bar{4}2$ and $\bar{2}\bar{8}2$ for the ($hk2$) layer, respectively. The gray and white arrows mark examples of the pressure-induced *odd-odd-even* and *even-odd-even* reflections whereas the white dashed arrows mark an example *even-even-even* reflection. The marked reflections are magnified on the right-hand side of the figure.

rhombohedral phase formed at $p_{c1} = 1.9$ GPa. Hence, in addition to the main perovskite reflections with h,k,l all even (*eee*), odd-odd-odd (*ooo*) superstructure reflections arising from antiphase BO_6 tilts are superimposed on the broad *ooo* reflections arising from the long-range CBO. The $a^-a^-a^-$ tilt pattern was verified by neutron powder diffraction.[30]

At 7.7 GPa two new classes of superstructure reflections appear, unambiguously revealing that a second pressure-induced phase transition occurs in PST with a critical pressure p_{c2} between 5.0 and 7.7 GPa. The first class of additional Bragg reflections has Miller indices of type h,k,l with one odd and two even (*oee*), while the second class has Miller indices of type h,k,l with two odd and one even (*ooe*). In terms of symmetry-adapted phonon modes in the Brillouin zone of the aristotype structure (primitive cubic single-perovskite $Pm\bar{3}m$), the *oee* reflections are associated with distortions driven by X-point (0, 1/2, 0) phonon modes of the cubic single-perovskite structure, whereas the *ooe* reflections are associated with activation of phonon modes on the M point (1/2, 1/2, 0).

The occurrence of a phase comprising only in-phase tilts would give rise to *ooe* (M-point) reflections.[46] The simultaneous observation of *ooo* (R-point) and *ooe* (M-point) Bragg reflections can be explained by a coexistence of two phases possessing respectively pure antiphase tilting [corresponding to a mode at the R point (1/2, 1/2, 1/2) in the primitive cubic cell] and pure in-phase tilting. However, this cannot explain the appearance of X-point Bragg peaks. Therefore, the simultaneous appearance of M-point and X-point reflections along with the existing R-point reflections could arise from three main types of transformation mechanism: (i) a change in the type of tilting from antiphase tilts only to mixed tilts (e.g., $a^+b^-b^-$), which would contribute to the R-point Bragg peaks and would give rise to both M- and X-point Bragg peaks;[47] (ii) development of a pattern of antipolar A-cation shifts consistent with an X-point mode,[48] which along with the preexisting antiphase tilts (associated with R-point modes) further lowers the symmetry and allows additional distortions (in-phase tilting along at least one direction or octahedral distortion) that would produce weak M-point reflections; (iii) simultaneous development of a tilt pattern involving in-phase tilting along at least one direction as well as an X-point pattern of A-cation shifts, which are consistent with each other.

The integrated intensities of the *oee* (X-point) reflections are systematically stronger than the intensities of the *ooe* (M-point) reflections. This unambiguously reveals the presence of long-range antipolar order of the A-site Pb atoms corresponding to an X-point distortion mode. A careful analysis of the diffraction patterns reveals that all X-point reflections of type $o00$ are absent. This indicates that the Pb cations must be displaced in opposite directions in consecutive (001) layers of the cubic structure, where the displacements within the (001) layers can be along any cubic $[uv0]$ direction. Examination of the symmetry of the possible displacement patterns with the program ISODISTORT[48] suggests that the X^{5+} mode (Miller-Love notation) provides the most physically reasonable arrangement of anti-ferrodistortive Pb displacements. Such a pattern of Pb displacements is inconsistent with pure in-phase tilt configurations[46] but it may coexist with a mixed octahedral tilt pattern. However, it is not possible either to confirm or to rule out a possible change in the type of tilting by structure refinements to the XRD data sets because of the oversaturation of the strongest Bragg peaks under experimental conditions necessary for the detection of the weak X- and M-point peaks.

From a pure-symmetry point of view, it is possible that the M-point Bragg peaks arise from A-site or B-site cation displacements.[48] However, the former would mean a coexistence of X-point and M-point Pb-displacement patterns, which is irrational, while the latter is inconsistent with the

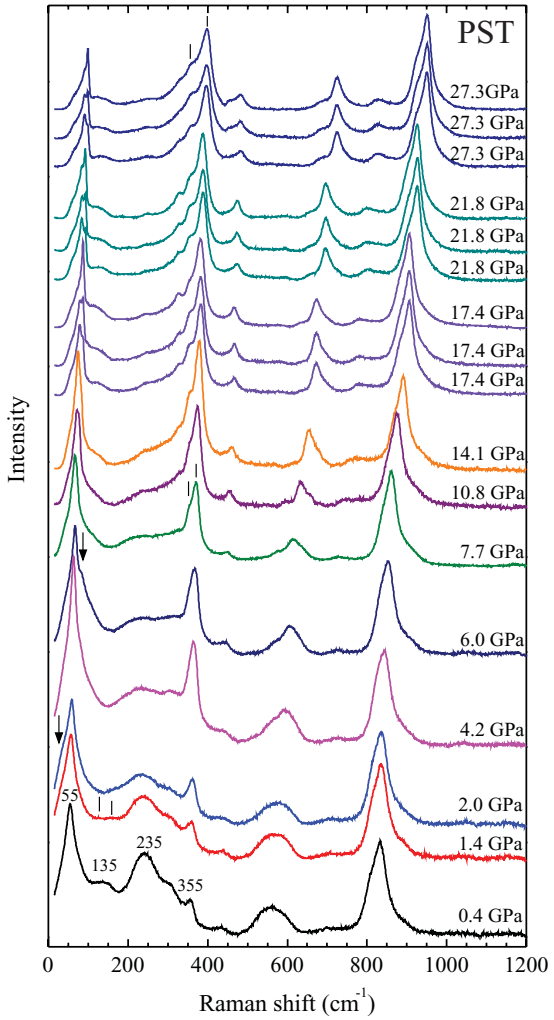

FIG. 3. (Color online) Raman spectra of PST at different pressures. The peak near 135 cm^{-1} is split above $p^{\star} = 1.2$ GPa; a soft mode near 35 cm^{-1} appears at $p_{c1} = 1.9$ GPa.[28] Spectra measured at the same pressure are from different spatial areas of the sample.

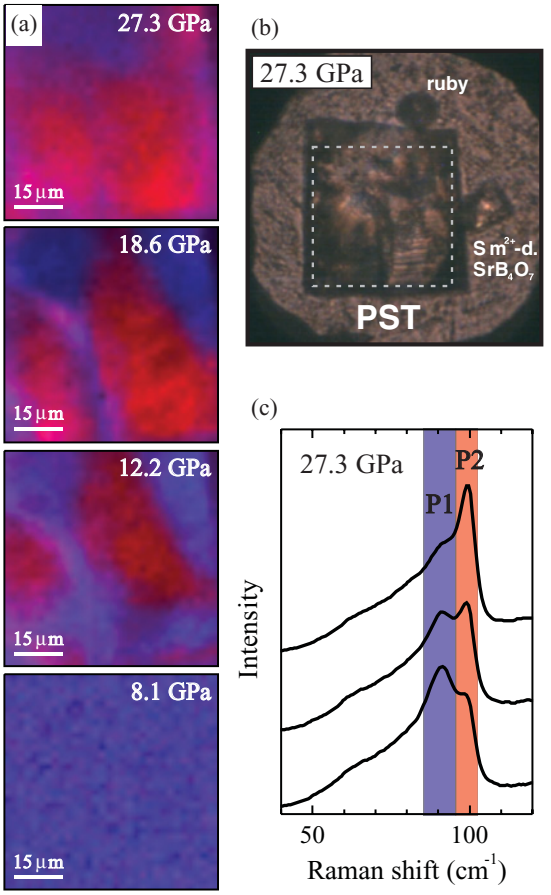

FIG. 4. (Color) Raman mappings (a) of single-crystal PST at different pressures based on the integrated intensity ratio between the signals P2 and P1 (c); red corresponds to large ratio $I(\mathrm{P2})/I(\mathrm{P1})$, blue to small ratio. The mapping area is marked by the white dashed square in the crystal image (b).

Raman scattering data (see Fig. 3), showing that the peak near 235 cm^{-1}, which results from off-centered B-site cations,[43,44] is strongly suppressed at high pressures.

Raman spectroscopy (see Fig. 3) also indicates that the most pronounced structural change above p_{c2} is a rearrangement of the Pb system. The major spectral changes above 6 GPa are in the band near 55 cm^{-1}, which is generated by Pb-localized phonon modes. At 6 GPa a new, sharp, higher-wave-number component appears to the main signal. At very high pressures (17.4 GPa and above) the Raman band arising from Pb vibrations is composed of several sharp signals and the intensity of the highest-wave-number component varies across the sample (see Figs. 3 and 4), while the Raman scattering above 110 cm^{-1} collected at the same pressure from different areas is almost the same (see Fig. 3). The variations in the intensity ratio of the Raman signals related to Pb vibrations is attributed to the coexistence of at least two configurations of Pb atoms, i.e., coexistence of two phases in the sample: the ferroic phase developed above p_{c1} and the ferroic phase developed above p_{c2}. The presence of a cubic phase ($Fm\bar{3}m$) along with the ferroic phases is also plausible, but definitely it is not the dominant phase at very high pressures because many more Raman peaks than the four peaks ($A_{1g} + E_g + 2F_{2g}$) allowed by symmetry in $Fm\bar{3}m$ are observed at 27.3 GPa.

The *oee* (X-point) and *ooe* (M-point) Bragg reflections are very weak or even disappear at 27.3 GPa (see Fig. 2). This might be an artificial effect due to the fact that the (hkl) layers have been reconstructed in a cubic metric while the ferroic distortion is very strong at this pressure, or it may indicate that the symmetry of the structure indeed becomes higher. The latter is however ruled out by the Raman data. Raman mapping [Fig. 4(a)] based on the ratio between the integrated intensities of the higher- and lower-wave-number major components generated by Pb vibrations [the peaks labeled in Fig. 4(c) as P2 and P1] reveal that with pressure increase the fraction of the ferroic phase developed above p_{c2} gradually increases and it is the dominant phase at 27.3 GPa.

Previously we have shown that the Raman peak near 355 cm^{-1} split in two at 3 GPa.[28] The Raman data up to 30 GPa show that the splitting increases with pressure [see Figs. 3 and 5(a)]. This Raman signal is related to the F_{2u} mode of the aristotype cubic structure and is generated by Pb-O bond stretching within the cubic {111} planes. This type of vibration can also be considered as octahedral tilting[43,44] and hence the peak is strongly enhanced above p_{c1}. The splitting of

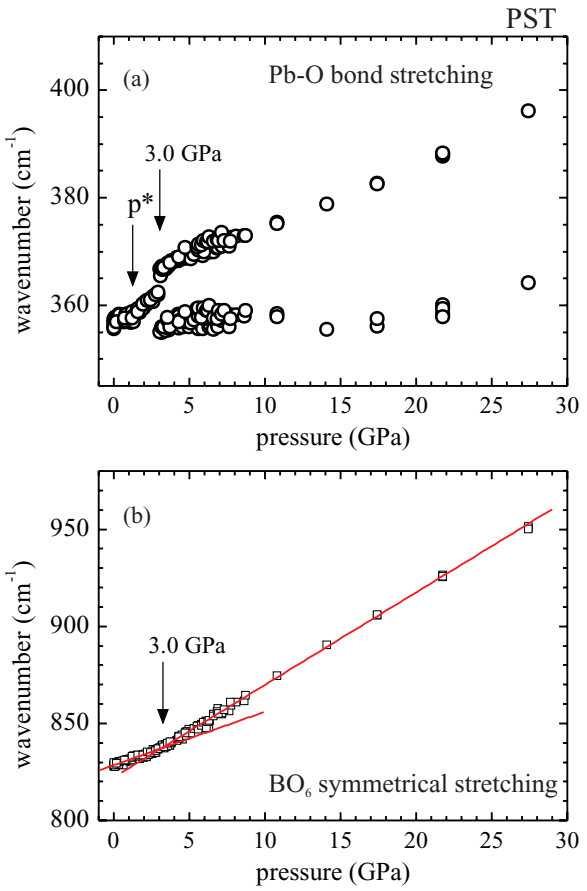

FIG. 5. (Color online) Pressure dependence of the wave number ω of the peak near 355 cm^{-1} (a) and 830 cm^{-1} (b) for PST; the uncertainties are within the symbols. The low-pressure data are after Mihailova *et al.*[28] The lines in the bottom plot are linear fits to the data points below p_{c1} and above p_{c2}, correspondingly.

the peak above 3 GPa indicates a lowering of symmetry of the oxygen cavity surrounding Pb and suggests that the BO_6 tilting around the cubic X, Y, and Z axes is no longer the same. The tilts may differ from each other in magnitude and/or type. The pressure evolution of the wave number of the BO_6 symmetrical stretching giving rise to the peak at 830 cm^{-1} [see Fig. 5(b)] also shows that the local structure is changed already at 3 GPa, i.e., below p_{c2}.

The appearance of a higher-wave-number component to the main Raman signal generated by Pb vibrations at 6 GPa indicates that p_{c2} is most probably between 5.0 and 6.0 GPa. This value corresponds well to our previous neutron powder diffraction data,[30] which at 5.5 GPa showed broadening of all diffraction peaks as well as a decrease in the magnitude of the anisotropic displacement ellipsoids refined in $R\bar{3}c$. The former should be due to unresolved splitting due to the lowering of the symmetry, while the latter is consistent with ordering of antiparallel Pb off-center displacements along the cubic $[uv0]$ directions. Neither *oee* (X-point) nor *ooe* (M-point) superstructure Bragg reflections could be observed in the neutron powder patterns up to 7.35 GPa. However, with regard to the intensity ratio $I(ooe)/I(ooo) \sim 1/6$ in the XRD patterns at 7.7 GPa as well as to the smaller Pb atomic form factors for neutrons, we would not expect to be able to detect these peaks above the background. The fact that *ooe* (M-point) superstructure Bragg peaks are not seen by neutron diffraction underlines that a change of the tilt system from antiphase to mixed, if any, is not the driving structural mechanism that leads to the second pressure-induced phase transition in PST.

At pressures of 14.1 GPa and above all classes of Bragg reflections observed by single-crystal synchrotron XRD (see Fig. 1) appear split. The splitting is due to a combination of the presence of multiple domains and an enhancement of the ferroic distortion arising from the phase transition at $p_{c2} \sim 5.5$ GPa. The splitting is only resolved at high pressures and its appearance does not imply the presence of a third pressure-induced phase transition.

Thus, a possible scenario for the structural transformations occurring in PST up to 30 GPa is as follows. At $p^\star = 1.2$ GPa the mesoscopic polar order is violated on the account of the development of local antipolar order of Pb cations and quasidynamical long-range order of antiphase BO_6 tilts of equal magnitude. At $p_{c1} = 1.9$ GPa a static $a^-a^-a^-$ tilt order is developed that leads to the occurrence of a continuous phase transition from cubic to nonpolar rhombohedral symmetry. At 3.0 GPa unequal octahedral tilts are locally developed. At $p_{c2} \sim 5.5$ GPa a second phase transition from rhombohedral to monoclinic or triclinic symmetry occurs, which involves a long-range order of Pb antipolar displacements along cubic $[uv0]$ directions and compatible rearrangements of the O atoms. Above p_{c2} the lower symmetry phase coexists with the nonpolar rhombohedral phase, as its fraction increases with increasing pressure.

C. The structural state of PSN up to 30 GPa

The reciprocal-space layer sections of PSN reconstructed in $Fm\bar{3}m$ from synchrotron single-crystal XRD are shown in Fig. 6. Since the PSN compound studied here possesses heavily frustrated CBO, the observed *ooo* (R-point) Bragg peaks result entirely from antiphase ($a^-a^-a^-$) tilts characteristic of the phase developed above $p_{c1} = 4.1$ GPa. New classes of pressure-induced Bragg peaks were not detected for PSN over the entire pressure range studied. Therefore, neither long-range order of A-cation antipolar shifts corresponding to X-point phonon modes nor in-phase octahedral tilts are developed in PSN up to 28.9 GPa.

The Raman spectra of PSN (see Fig. 7) also do not show any evidence for the development of long-range order of antipolar Pb off-center shifts. At 24.9 and 28.9 GPa, the Raman band near 50 cm^{-1} can be rationally fitted with three components, but these components are very broad as compared to the corresponding Raman signals for PST, indicating that the structural changes that occur are only local. Spectra collected at the same pressure from different spatial areas of the PSN sample reveal that the sample remained structurally homogeneous in the entire pressure range studied. A splitting of the peak near 350 cm^{-1} at 10.1 GPa [Figs. 7 and 8(a)] can be deduced from the spectrum profile fittings, which suggests that on the local scale the octahedral tilts around the cubic [100], [010], and [001] become different. The position of the peak near 815 cm^{-1}, which arises from the BO_6 symmetrical stretching, has a kink as a function of pressure at 7.1 GPa [see

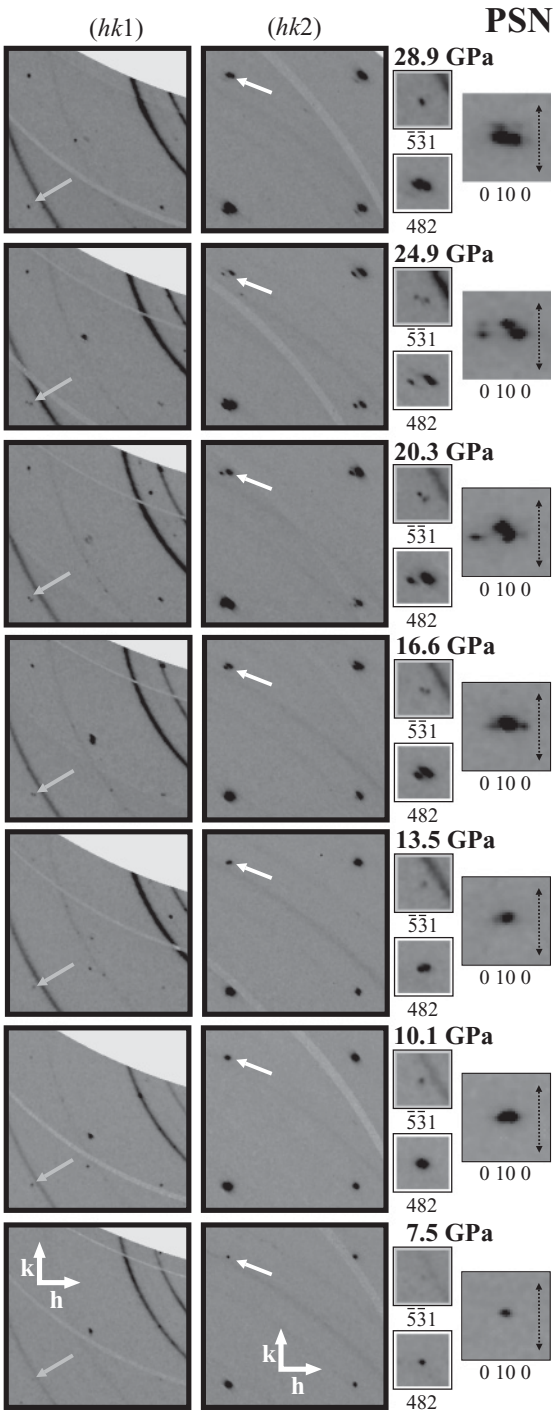

FIG. 6. Reciprocal-space layer sections of PSN reconstructed in $Fm\bar{3}m$ from single-crystal synchrotron XRD data at different pressures. The reflection in the lower-left and upper-right corners are $\bar{5}\bar{1}1$ and $\bar{3}\bar{3}1$ for the ($hk1$) layer and 482 and 662 for the ($hk2$) layer, respectively. The gray and white arrows mark examples of the pressure-induced *odd-odd-odd* and *even-even-even* reflections, which are shown on an enlarged scale. The 0 10 0 reflection is also shown; the black vertical arrows in the 0 10 0-layer sections mark the direction to the coordinate origin.

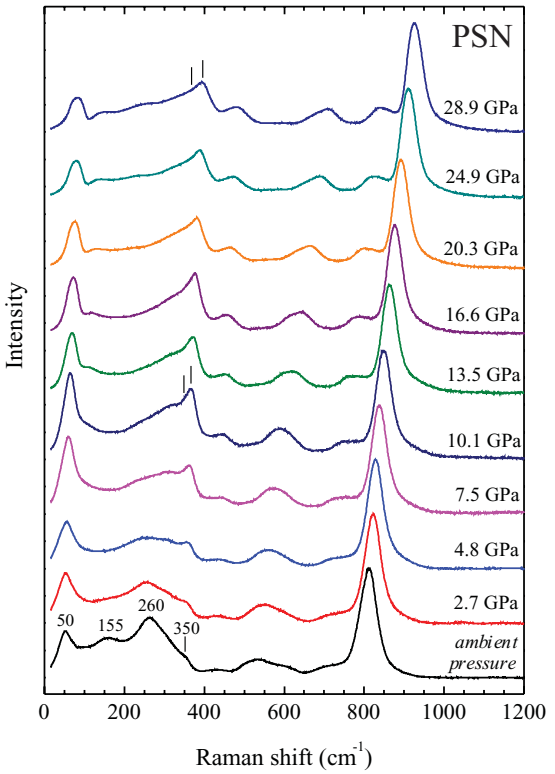

FIG. 7. (Color online) Raman spectra of PSN at different pressures.

Fig. 8(b)]. Therefore, the Raman data indicate the occurrence of local structure changes in the pressure range 7–10 GPa, which involve a lowering of the symmetry of the octahedral tilt patterns and might precede a phase transition.

At pressures above 10.1 GPa all Bragg reflections split (see Fig. 6), which however could result solely from the increasing rhombohedral distortion of the unit cell and the development of the multidomain rhombohedral structure. Only splitting of diffraction peaks of type $e00$ would indicate a deviation of the symmetry of the average structure from rhombohedral. Besides, in the case of single-crystal diffraction the splitting should be along the direction to the coordinate origin corresponding to different d spacings; splitting perpendicular to the direction to the coordinate is due to twinning. As an example of an $e00$-type reflection, Fig. 6 displays the 0 10 0 Bragg reflection: At 16.6 GPa the diffraction spot looks asymmetric along the direction to the coordinate axis, whereas at higher pressure a splitting corresponding to different d spacings is noticeable. This indicates that the symmetry of the average structure is lowered from rhombohedral with a tilt system $a^-a^-a^-$ to monoclinic or triclinic, consistent with a tilt system $a^-b^-b^-$ or $a^-b^-c^-$, respectively.

Thus, at $p^\star$ and p_{c1} PSN undergoes the same structural transformations as PST. However the second phase transition of PSN at $p_{c2} \sim 16.6$ GPa differs from that of PST and it consists only of lowering of the antiphase-tilt pattern symmetry. The difference between the structural states of PST and PSN above p_{c2} is most probably related to the degree of local Pb displacive order developed at $p^\star$, which in turn should be related to the degree of frustrated chemical B-site order. The phase transitions observed for PSN up to 30 GPa are consistent with the first two pressure-induced phase transitions in PZN proposed by Janolin *et al.*[23]

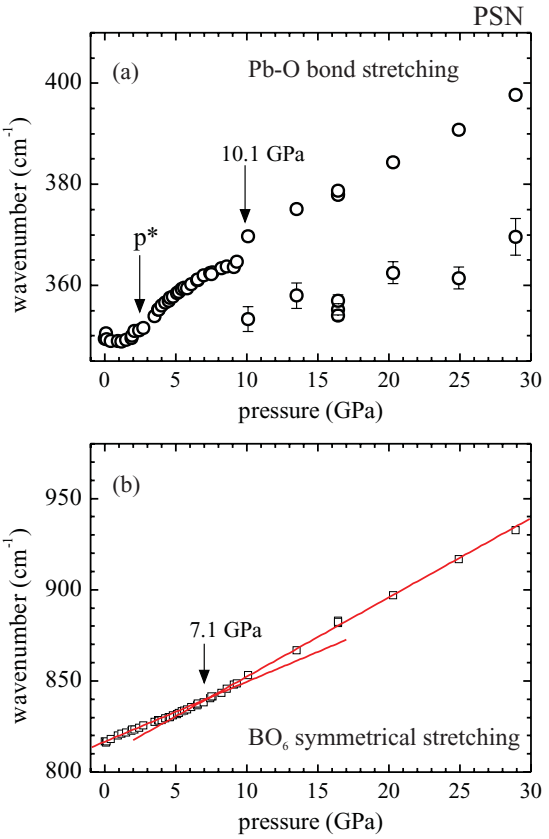

FIG. 8. (Color online) Pressure dependence of the wave number ω of the peak near 355 cm^{-1} (a) and 830 cm^{-1} (b) for PSN; the uncertainties are within the symbols. The low-pressure data are after Welsch *et al.*[29] The lines in the bottom plot are linear fits to the data points below p_{c1} and above p_{c2}, respectively.

D. DFT calculations on PST and PSN

The results of our DFT calculations obtained for PST and PSN are shown in Figs. 9 and 10, respectively. The figures display the total energy E (per $A_2B'B''O_6$ formula unit) as a function of the unit-cell volume [Figs. 9(a) and 10(a)], the volume dependence of the total energy relative to $I4/m$, i.e., $E(V) - E_{I4/m}(V)$ [Figs. 9(b) and 10(b)], and the pressure dependence of the enthalpy $H = E + pV$, also taken relative to $I4/m$, i.e., $H(p) - H_{I4/m}(p)$ [Figs. 9(c) and 10(c)]. These relative energies and enthalpies better reveal the small differences between the structures with nonzero tilts. The $a^-b^-b^-$ structure is not included in the plots, because the corresponding structures relax to $a^0b^-b^-$. The enthalpies relative to $I4/m$ were evaluated as follows: First the $H(p)$ data for $I4/m$ was fitted by a quadratic polynomial, and then $H_{I4/m}$ for the pressure values of the other tilt configurations was calculated from the polynomial fit in order to subtract the $H(p)$ of $I4/m$ from the $H(p)$ data set of the corresponding structure.

It is apparent that for both compounds essentially the same trends are observed; i.e., the difference in the electronic structure of Ta and Nb should not have any impact on the type of observed structural transformations. According to the DFT calculations, all non-zero-tilt systems are much more stable than the cubic structure [see Figs. 9(a) and

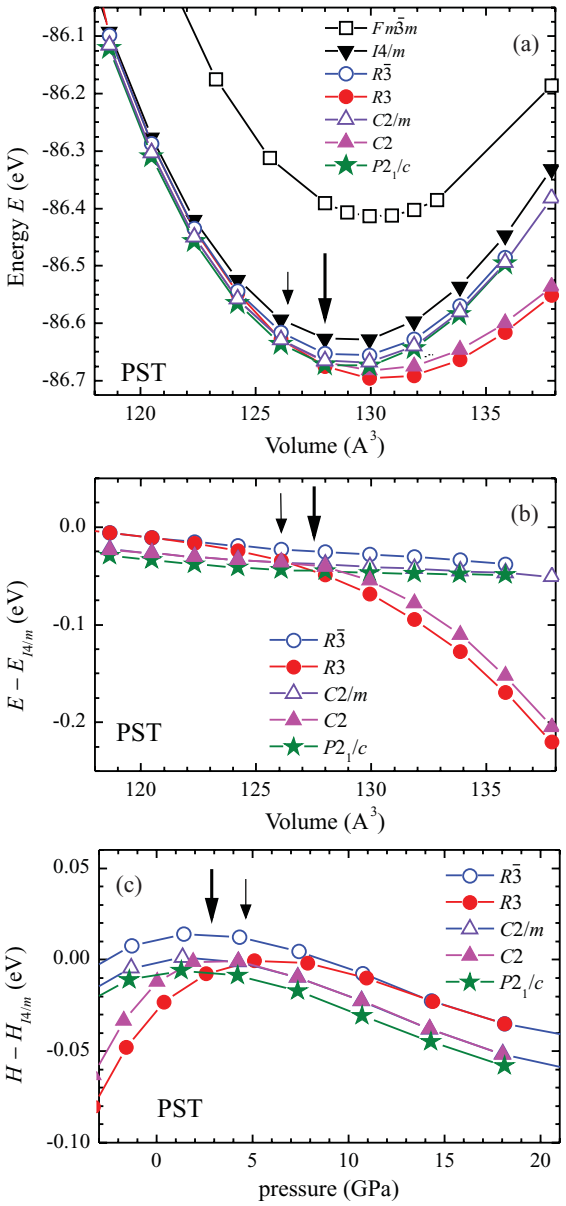

FIG. 9. (Color online) Results of DFT calculations on PST with perfect chemical 1:1 B-site order: Total energy versus volume (a), total energy relative to $I4/m$ ($E - E_{I4/m}$) versus volume (b), and enthalpy H relative to $I4/m$ ($H - H_{I4/m}$) versus pressure (c). All energies, enthalpies, and volumes correspond to one $A_2B'B''O_6$ formula unit. The thin arrows point to a phase transition from polar $a^-a^-a^-$ structure to nonpolar or polar $a^0b^-b^-$ structure. The bold arrows point to a phase transition from polar $a^-a^-a^-$ structure to nonpolar $a^+b^-b^-$ structure.

10(a)]. Among the tilted configurations, $a^-b^0b^0$ ($I4/m$) is the most energetically unfavorable within the whole volume (i.e., pressure) range. This is in agreement with the Rietveld refinements to neutron diffraction data on PST and PSN, which showed that this tilt system represents the poorest fit to the diffraction data.[30,32] Among the nonpolar structures with antiphase tilts, $a^0b^-b^-$ ($C2/m$), which can be considered as an end member of $a^-b^-b^-$, $a < b$, is energetically most stable (see Figs. 9 and 10). At larger volumes (lower pressures) the polar structures are energetically preferred and the $R3$

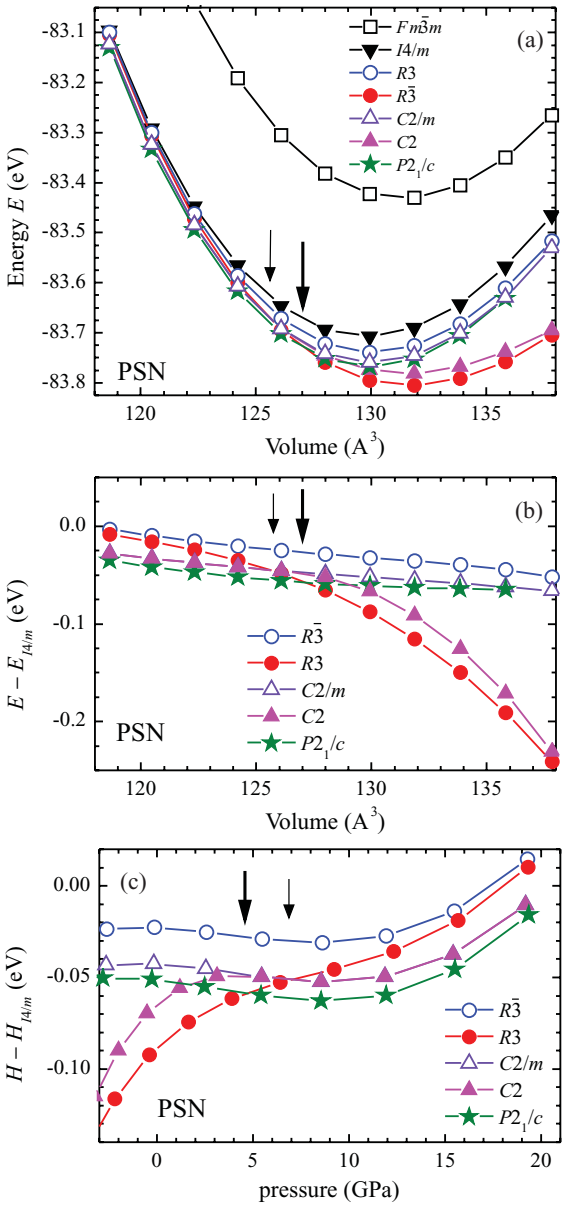

FIG. 10. (Color online) Results of DFT calculations on PSN with perfect chemical 1:1 B-site order: Total energy versus volume (a), total energy relative to $I4/m$ ($E - E_{I4/m}$) versus volume (b), and enthalpy H relative to $I4/m$ ($H - H_{I4/m}$) versus pressure (c). All energies, enthalpies, and volumes correspond to one $A_2B'B''O_6$ formula unit. The thin arrows point to a phase transition from polar $a^-a^-a^-$ structure to nonpolar or polar $a^0b^-b^-$ structure. The bold arrows point to a phase transition from polar $a^-a^-a^-$ structure to nonpolar $a^+b^-b^-$ structure.

space group is the most stable. This is consistent with the experimentally determined low-temperature structure of PST with partial chemical order.[49] Near the minimum of the energy-versus-volume plot for $R3$, the calculated off-centered displacements of Pb^{2+}, B^{3+}, and B^{5+} with respect to the center of gravity of the surrounding oxygen atoms are ≈0.37, 0.08, and 0.07 Å in the case of PST ($V = 129.9$ Å^3, $p = 0.4$ GPa) and ≈0.38, 0.09, and 0.09 Å in the case of PSN ($V = 129.9$ Å^3, $p = 1.6$ GPa). These values are in good agreement with the B-cation and Pb off-centered shifts estimated from x-ray absorption and nuclear magnetic resonance spectroscopy.[45,50] If we restrict our considerations only to antiphase tilt systems, a pressure-induced phase transition from a polar structure with $a^-a^-a^-$ tilt pattern to a nonpolar or polar structure with $a^0b^-b^-$ tilt pattern is deduced from the DFT calculations. At very high pressures the polar and nonpolar counterparts of the same tilt configurations become energetically indistinguishable, implying that the polar shifts are gradually suppressed with increasing pressure, and essentially become zero at very high pressure. For example, in the case of PST, $R3$ at $p = 18.1$ GPa ($V = 118.6$ Å^3), the polar cation displacements with respect to the centers of the surrounding oxygen cavities for Pb^{2+}, B^{3+}, and B^{5+} are ≈0.03, 0.005, and 0.004 Å, i.e., practically zero. For PSN with $R3$ at $p = 19.3$ GPa ($V = 118.6$ Å^3) the off-centered displacements of Pb^{2+}, B^{3+}, and B^{5+} are a bit larger, ≈0.17, 0.04, and 0.04 Å. One should also keep in mind that the calculations represent structures at 0 K and low temperatures naturally enhance the polar order in perovskite-type ferroelectrics, while the *in situ* high-pressure experiments have been performed at room temperature. Hence, the stability of polar order under pressure is "overestimated" in the calculations as compared to the room-temperature stability, which is actually measured in high-pressure experiments.

According to the DFT calculations, the energetically most favorable tilt configuration at high pressures is $a^+b^-b^-$, with mixed in-phase/antiphase tilts. Close examination of the atomic positions of the relaxed structures reveal that this mixed-tilt configuration ($P2_1/c$) comprises considerable X^{5+}-mode-driven Pb displacements, 0.1 Å for both PST and PSN, within the whole volume range of 129.9–118.6 Å^3, which corresponds to a pressure range of 4.2–18.1 GPa for PST and of 5.4–19.3 GPa for PSN. The other tilt configurations studied by DFT calculations produce smaller Pb displacements, which are associated with an R^{5+} mode and hence will contribute to the *ooo* (R-point) Bragg peaks and not to the *ooe* (M-point) diffraction peaks observed above p_{c2}. Therefore, the combined analysis of the experimental and DFT-calculation results show that the tilt system changes from purely antiphase to mixed only if anti-ferrodistortive long-range order of Pb atoms triggered by an X^{5+} mode occurs at high pressures. If for some reason such a displacive long-range order of the Pb cations does not take place, the pressure increase leads only to a lowering of the symmetry of the antiphase tilt configuration from $a^-a^-a^-$ to $a^0b^-b^-$. It is worth noting that at ambient pressure the $a^+b^-b^-$ tilt system is the most commonly observed for perovskite-type materials, and it has been proposed that this is due to the fact that the $a^+b^-b^-$ tilting tends to maximize the A-O covalent bonding and minimize the A-O repulsive overlap.[51] Our results suggest that the same arguments may be applicable for the high-pressure state of other perovksite-type materials with A-site cations showing affinity to off-centering and heterovalent cations on the B site.

V. CONCLUSIONS

In the pressure range up to 30 GPa, two phase transitions are observed in both PST and PSN. The phase transitions

are preceded by characteristic pressures at which the local symmetry is changed. Thus, one can propose four important pressure points typical of Pb-based perovskite-type relaxors: (i) the characteristic pressure $p_1^\star$, at which the off-centered Pb and B cations in PNRs decouple, while local antipolar order of Pb cations as well as quasidynamical long-range order of antiphase BO_6 tilts of equal magnitude are developed; (ii) the critical pressure p_{c1} at which a continuous phase transition from a relaxor-cubic to a nonpolar rhombohedral state occurs, as the primary order parameter is antiphase $a^-a^-a^-$ tilt order; (iii) the characteristic pressure $p_2^\star$ at which the octahedral tilts around the cubic [100], [010], and [001] directions become different from each other on the local scale; (iv) the critical pressure p_{c2} at which a second phase transition from nonpolar rhombohedral to nonpolar monoclinic or triclinic symmetry occurs. The latter phase transition involves long-range-ordered antiphase tilts with unequal magnitudes ($a^0b^-b^-$) without Pb displacement ordering or a long-range order of Pb antipolar displacements along cubic [$uv0$] directions and a compatible mixed tilt system ($a^+b^-b^-$). The characteristic and critical pressures for the tantalate compound are lower than the corresponding values for the niobate compound, similarly to the critical temperatures of the paraelectric-to-ferroelectric phase transition.[52]

Although PST and PSN have the same stoichiometry and tolerance factor, the degree of frustrated CBO in PST is slightly higher than in PSN; i.e., PST exhibits a longer coherence length between B′-O-B″ linkages. This is most probably the reason why the intrinsic coherence of ferroic Pb-O species existing at ambient pressure is more pronounced in PST than in PSN. The degree of frustrated CBO and coherent ferroic Pb-O species strongly influences the structural state at $p_1^\star$ and consequently the nature of the structural transformations at p_{c2}.

The DFT-calculation results indicate that for Pb-based relaxors with a complete 1:1 chemical B-site order structures with nonzero octahedral tilting are considerably more stable than the untilted structure.

Up to 30 GPa, no experimental evidence for the occurrence of a polar state involving nucleus ferroic order was detected. DFT calculations also show that the polar distortion gradually decreases with increasing pressure and near 20 GPa should be negligibly small. The pressure-induced decoupling between off-centered shifts of Pb and B cations in polar nanoregions that occur at $p_1^\star$ triggers the development of anti-ferrodistortive long-range order. This suggests that at ambient pressure and room temperature the polar and anti-ferrodistortive order coexist on the mesoscopic scale and this might be the reason for the relaxor state.

ACKNOWLEDGMENTS

Financial support by the Deutsche Forschungsgemeinschaft (MI 1127/2-2, INST 152/460-1, and INST 152/526-1), National Science Foundation (EAR-0738692), and Science Foundation Ireland (SFI-07/YI2/I1051) is gratefully acknowledged. The authors thank Björn Winkler, Goethe-Universität Frankfurt, for the opportunity to use the He-gas loading setup available in his laboratory.

*boriana.mihailova@uni-hamburg.de
†rangel@vt.edu

[1] A. A. Bokov and Z.-G. Ye, J. Mater. Sci. **41**, 31 (2006).
[2] J. F. Scott, Science **315**, 954 (2007).
[3] M. D. Glinchuk, E. A. Eliseev, V. A. Stephanovich, E. V. Kirichenko, and L. Jastrabik, Appl. Phys. Lett. **80**, 646 (2002).
[4] A. Bussmann-Holder, A. R. Bishop, and T. Egami, Europhys. Lett. **71**, 249 (2005).
[5] B. P. Burton, E. Cockayne, S. Tinte, and U. V. Waghmare, Phase Transitions **79**, 91 (2006).
[6] J. Hlinka, T. Ostapchuk, D. Noujni, S. Kamba, and J. Petzelt, Phys. Rev. Lett. **96**, 027601 (2006).
[7] W. Kleemann, Annu. Rev. Mater. Res. **37**, 415 (2007).
[8] P. Ganesh, E. Cockayne, M. Ahart, R. E. Cohen, B. Burton, R. J. Hemley, Y. Ren, W. Yang, and Z.-G. Ye, Phys. Rev. B **81**, 144102 (2010).
[9] D. Fu, H. Taniguchi, M. Itoh, S.-y. Koshihara, N. Yamamoto, and S. Mori, Phys. Rev. Lett. **103**, 207601 (2009).
[10] G. Xu, J. Phys. Soc. Jpn. **79**, 011011 (2010).
[11] R. Blinc, A. Gregorovič, B. Zalar, R. Pirc, V. V. Laguta, and M. D. Glinchuk, Phys. Rev. B **63**, 024104 (2000).
[12] B. Mihailova, B. Maier, C. Paulmann, T. Malcherek, J. Ihringer, M. Gospodinov, R. Stosch, B. Güttler, and U. Bismayer, Phys. Rev. B **77**, 174106 (2008).
[13] G. Burns and F. H. Dacol, Phys. Rev. B **28**, 2527 (1983).
[14] J. Toulouse, F. Jiang, O. Svitelskiy, W. Chen, and Z. G. Ye, Phys. Rev. B **72**, 184106 (2005).
[15] E. Dul'kin, M. Roth, P.-E. Janolin, and B. Dkhil, Phys. Rev. B **73**, 012102 (2006).
[16] B. Dkhil, P. Gemeiner, A. Al-Barakaty, L. Bellaiche, E. Dul'kin, E. Mojaev, and M. Roth, Phys. Rev. B **80**, 064103 (2009).
[17] N. Takesue, Y. Fujii, M. Ichihara, and H. Chen, Phys. Rev. Lett. **82**, 3709 (1999).
[18] I. W. Chen, J. Phys. Chem. Solids **61**, 197 (2000).
[19] N. Waeselmann, B. Mihailova, B. J. Maier, C. Paulmann, M. Gospodinov, V. Marinova, and U. Bismayer, Phys. Rev. B **83**, 214104 (2011).
[20] B. J. Maier, A.-M. Welsch, B. Mihailova, R. J. Angel, J. Zhao, C. Paulmann, J. M. Engel, W. G. Marshall, M. Gospodinov, D. Petrova, and U. Bismayer, Phys. Rev. B **83**, 134106 (2011).
[21] A. M. Glazer, Acta Crystallogr. Sect. B **28**, 3384 (1972).
[22] B. Mihailova, R. J. Angel, B. J. Maier, A.-M. Welsch, J. Zhao, M. Gospodinov, and U. Bismayer, IEEE Trans. Ultrason. Ferroelectr. Freq. Control **58**, 1905 (2011), and references therein.
[23] P. E. Janolin, B. Dkhil, P. Bouvier, J. Kreisel, and P. A. Thomas, Phys. Rev. B **73**, 094128 (2006).
[24] B. Chaabane, J. Kreisel, B. Dkhil, P. Bouvier, and M. Mezouar, Phys. Rev. Lett. **90**, 257601 (2003).
[25] I. A. Kornev, L. Bellaiche, P. Bouvier, P.-E. Janolin, B. Dkhil, and J. Kreisel, Phys. Rev. Lett. **95**, 196804 (2005).
[26] R. J. Angel, M. Bujak, J. Zhao, G. D. Gatta, and S. D. Jacobsen, J. Appl. Crystallogr. **40**, 26 (2007).
[27] S. Klotz, J.-C. Chervin, P. Munsch, and G. Le Marchand, J. Phys. D: Appl. Phys. **42**, 075413 (2009).

[28]B. Mihailova, R. J. Angel, A.-M. Welsch, J. Zhao, J. Engel, C. Paulmann, M. Gospodinov, H. Ahsbahs, R. Stosch, B. Güttler, and U. Bismayer, Phys. Rev. Lett. **101**, 017602 (2008).
[29]A.-M. Welsch, B. Mihailova, M. Gospodinov, R. Stosch, B. Güttler, and U. Bismayer, J. Phys. Condens. Matter **21**, 235901 (2009).
[30]B. J. Maier, R. J. Angel, W. G. Marshall, B. Mihailova, C. Paulmann, J. M. Engel, M. Gospodinov, A.-M. Welsch, D. Petrova, and U. Bismayer, Acta Crystallogr. Sect. B **66**, 280 (2010).
[31]B. J. Maier, A.-M. Welsch, R. J. Angel, B. Mihailova, J. Zhao, J. M. Engel, L. A. Schmitt, C. Paulmann, M. Gospodinov, A. Friedrich, and U. Bismayer, Phys. Rev. B **81**, 174116 (2010).
[32]B. J. Maier, R. J. Angel, B. Mihailova, W. G. Marshall, M. Gospodinov, and U. Bismayer, J. Phys. Condens. Matter **23**, 035902 (2011).
[33]R. Boehler, Rev. Sci. Instrum. **77**, 115103 (2006).
[34]R. Munro, G. Piermarini, S. Block, and W. Holzapfel, J. Appl. Phys. **57**, 165 (1985).
[35]F. Datchi, A. Dewaele, P. Loubeyre, R. LeToullec, Y. Le Godec, and B. Canny, High Press. Res. **27**, 447 (2007).
[36]R. O. Jones and O. Gunnarsson, Rev. Mod. Phys. **61**, 689 (1989).
[37]G. Kresse and J. Furthmüller, Comput. Mater. Sci. **6**, 15 (1996).
[38]P. E. Blöchl, Phys. Rev. B **50**, 17953 (1994).
[39]G. Kresse and D. Joubert, Phys. Rev. B **59**, 1758 (1999).
[40]R. D. Shannon, Acta Crystallogr. Sect. A **32**, 751 (1976).
[41]C. G. F. Stenger and A. J. Burggraaf, Phys. Status Solidi **61**, 275 (1980).
[42]B. J. Maier, B. Mihailova, C. Paulmann, J. Ihringer, M. Gospodinov, R. Stosch, B. Güttler, and U. Bismayer, Phys. Rev. B **79**, 224108 (2009).
[43]B. Mihailova, U. Bismayer, B. Güttler, M. Gospodinov, and L. Konstantinov, J. Phys. Condens. Matter **14**, 1091 (2002).
[44]A.-M. Welsch, B. J. Maier, B. Mihailova, R. J. Angel, J. Zhao, C. Paulmann, J. M. Engel, M. Gospodinov, V. Marinova, and U. Bismayer, Z. Kristallogr. **226**, 126 (2011).
[45]A. I. Frenkel, D. M. Pease, J. Giniewicz, E. A. Stern, D. L. Brewe, M. Daniel, and J. Budnick, Phys. Rev. B **70**, 014106 (2004).
[46]C. J. Howard, B. J. Kennedy, and P. M. Woodward, Acta Crystallogr. Sect. B **59**, 463 (2003).
[47]D. I. Woodward and I. M. Reaney, Acta Crystallogr. Sect. B **61**, 387 (2005).
[48]B. J. Campbell, H. T. Stokes, D. E. Tanner, and D. M. Hatch, J. Appl. Crystallogr. **39**, 607 (2006).
[49]P. M. Woodward and K. Z. Baba-Kishi, J. Appl. Crystallogr. **35**, 233 (2002).
[50]D. H. Zhou, G. L. Hoatson, R. L. Vold, and F. Fayon, Phys. Rev. B **69**, 134104 (2004).
[51]P. M. Woodward, Acta Crystallogr. Sect. B **53**, 44 (1997).
[52]M. E. Lines and A. M. Glass, *Principles and Applications of Ferroelectrics and Related Materials* (Clarendon Press, Oxford, 1977).